Evanescent-wave proton postaccelerator driven by intense THz pulse

L. Pálfalvi,[1*] J. A. Fülöp,[2,3] Gy. Tóth,[1] and J. Hebling[1,2]

[1]*Department of Experimental Physics, University of Pécs, 7624 Pécs, Hungary*
[2]*MTA-PTE High-Field Terahertz Research Group, 7624 Pécs, Hungary*
[3]*ELI-Hu Nkft., 6720 Szeged, Hungary*

(Received 15 February 2013; revised manuscript received 27 November 2013; published 11 March 2014)

Hadron therapy motivates research dealing with the production of particle beams with ~100 MeV/nucleon energy and relative energy fluctuation on the order of 1%. Laser-driven accelerators produce ion beams with only tens of MeV/nucleon energy and an extremely broad spectra. Here, a novel method is proposed for postacceleration and monochromatization of particles, leaving the laser-driven accelerator, by using intense THz pulses. It is based on further developing the idea of using the evanescent field of electromagnetic waves between a pair of dielectric crystals. Simple model calculations show that the energy of a proton bunch can be increased from 40 to 56 MeV in five stages and its initially broad energy distribution can be significantly narrowed down.

DOI: 10.1103/PhysRevSTAB.17.031301 PACS numbers: 41.75.Jv, 41.75.Lx, 42.65.−k

I. INTRODUCTION

The development of particle accelerators is strongly motivated by medical applications, such as hadron therapy. Damaging tumor cells requires a collimated beam of monoenergetic (monochromaic) ions with 70 to 250 MeV/nucleon energy [1,2]. When such a beam interacts with (human) tissue, most of its energy is lost at a well-defined depth determined by the initial ion energy, and the ions damage the tissue predominantly at this depth. This method is much more selective than using γ rays, where the dose density is proportional to the intensity and decreases exponentially with the penetration depth. However, the few microwave ion accelerators, being in medical application worldwide, are large-scale facilities with extremely high operational costs. This makes the wide-spread application of hadron therapy difficult.

Alternatively, ion beams can also be produced by irradiating solid [3–7] or gas [8] targets by short laser pulses with typical intensities of 10^{20} W/cm^2, delivered by compact high-power laser systems. The highest so far proton energy reported from a laser-driven proton accelerator (LDPA) with a solid target is 58 MeV [3], which is the high-energy edge of an extremely broad energy spectrum. Additionally, the particle beam has large divergence. Focusing quadrupole magnets [9,10] or laser-driven microlenses [11,12] were used for beam collimation, which only increase the spatial concentration of protons belonging to a narrow energy band. Since the energy distribution of the protons remains constant, this only means narrow-band filtering rather than real monochromatization. By using a train of multi-terawatt CO_2 laser pulses interacting with a gas jet, proton beams with 20 MeV energy and an extremely narrow relative energy spread of about 1% were achieved [8]. However, besides the low proton energy, strong shot-to-shot energy fluctuation hinders (medical) application of this source.

Monoenergetic proton beams with sufficient energy for hadron therapy cannot be achieved directly by laser-based accelerators today. Even though conventional (microwave) accelerator technology could, in principle, be suitable for postacceleration of ions generated by laser-based ion sources, the use of such large-scale devices would abandon the main advantage of laser-based sources: their compactness. Recently, a more compact microwave accelerator, the side-coupled drift tube linac was proposed [13,14].

Another compact, laser-based postaccelerator was proposed for electron bunches [15], which uses the evanescent field in the vacuum gap between closely spaced dielectric materials. However, the use of visible or near-infrared laser pulses is not feasible, since the penetration depth of the evanescent field scales with the wavelength, and free propagation of particle beams requires at least a 50 μm gap size. Efficient acceleration also requires precise synchronization between the particle and the accelerating field: the velocity of the field should be adjusted to the instantaneous velocity of the particle. Reference [15] does not address synchronization issues. Solutions like varying either the refractive index of the medium, or the angle of incidence, or making the interface surface curved are impractical especially in the case of microwaves because of their long wavelength [16].

In this paper we propose a compact, entirely laser-based method for both postacceleration and monochromatization of the proton beam produced by a LDPA in order to make

*palfalvi@fizika.ttk.pte.hu

such sources suitable for hadron therapy. The proposed method, similarly to Refs. [15,16], uses the evanescent field for acceleration. The essential improvement is to use intense THz pulses undergoing total internal reflection at a dielectric-vacuum interface. The few-hundred μm wavelength of THz pulses naturally fits to typical sizes of proton beams, and focusing THz radiation by centimeter-sized optics is easy. The proposed method requires (near-)single-cycle pulses with a mean frequency around 1 THz and peak electric field strength of at least 1 MV/cm over a few centimeters distance. The THz pulse can be generated by the same laser pulse used for driving the LDPA. Besides its compactness, this integrated solution inherently provides accurate synchronization between the preaccelerated particle bunch and the postaccelerating THz field. Important details of synchronization will also be addressed, namely, the adequate setting of parameters such as the initial phase between the accelerating field and the particle, the phase velocity of the accelerating field, and the acceleration length.

The development of intense pulsed THz sources has witnessed a tremendous progress during the last decade. With the proposal of tilted-pulse-front pumping (TPFP), efficient optical rectification of femtosecond laser pulses in highly nonlinear materials, such as $LiNbO_3$ (LN), became available [17]. Since then, this technique has been providing the highest THz pulse energies ever achieved with table–top sources [18–20], recently reaching 125 μJ [20], and also the highest conversion efficiencies [21]. Up to 1 MV/cm peak electric field strength was reported [22] by focusing lower-energy pulses with about 1 THz mean frequency. Further substantial increase can be expected both in terms of THz pulse energy as well as peak electric field strength by using optimal pump pulse duration [23], cooling the LN crystal [23], and using the contact grating technique [24] for TPFP to allow a large pumped area. It can be expected in the near future that THz pulses with mJ-level energy in the 0.1–1 THz frequency range will be available from TPFP sources driven by sub-Joule-class efficient diode-pumped solid-state lasers, making the construction of compact proton postaccelerators feasible.

The paper is organized as follows. In Sec. II, we first describe the THz evanescent-wave proton postaccelerator and the accelerating electromagnetic field. Then, the acceleration of a single proton is analyzed both in the case of single and multiple accelerator stages. In Sec. III, the acceleration of proton bunches is discussed. Section IV contains a brief summary.

II. THE THZ EVANESCENT-WAVE PROTON POSTACCELERATOR

A. The accelerating field

The scheme of the THz-driven evanescent-wave accelerator is shown in Fig. 1. Protons with an initial velocity v_0 in the x direction enter the vacuum gap between the two symmetrically arranged dielectric prisms with refractive index n. The accelerating evanescent field in the gap is generated by two identical and synchronized THz pulses, both impinging on the vacuum-dielectric interfaces at the same angle of incidence $\alpha \geq \alpha_c$, with $\alpha_c = \arcsin(1/n)$ being the critical angle for total internal reflection. Assuming p polarization for the incident THz waves, the electric and the magnetic fields in the vacuum gap are given by the following expressions [15]:

$$\begin{aligned}\mathbf{E}(x,z,t) &= E_{\mathrm{in},0}\frac{\tau}{1-\rho e^{-kd\xi}}\times\left\{\mathbf{e}_x i\xi\left[\exp\left(k\left(z-\frac{d}{2}\right)\xi\right)+\exp\left(-k\left(z+\frac{d}{2}\right)\xi\right)\right]-\mathbf{e}_z n\sin\alpha\left[\exp\left(-k\left(z+\frac{d}{2}\right)\xi\right)\right.\right.\\ &\left.\left.-\exp\left(k\left(z-\frac{d}{2}\right)\xi\right)\right\}\times\exp[i(nky\sin\alpha-\omega t)],\\ \mathbf{B}(x,z,t) &= -\mathbf{e}_y\frac{1}{cn\sin\alpha}E_z(x,z,t).\end{aligned} \tag{1}$$

Here, $\xi=\sqrt{n^2\sin^2\alpha-1}$, $\gamma=\frac{n\xi}{\cos\alpha}$, $\rho=\exp(-2i\tan^{-1}\gamma)$, $\tau=\frac{2n}{1+i\gamma}$, k is the magnitude of the wavevector in vacuum, and $E_{\mathrm{in},0}$ is the amplitude of the electric field inside the dielectric. Except the symmetry plane, the electric field of the evanescent wave has both a parallel (x) and a perpendicular (z) component to the interface. While the x component of the electric field is responsible for particle acceleration, E_z and B_y exert a deflecting transversal force $F_z = q(E_z - vB_y)$, with v being the proton velocity, and q being the proton charge. F_z, which is out of phase by 90° relative to the longitudinal electric field component, can lead to focusing or defocusing of the proton beam. In the (x,y) symmetry plane the electric field has only an x component, and the magnetic field vanishes. The phase velocity of the evanescent wave parallel to the interface is $v_{\mathrm{THz}} = c/n\sin(\alpha)$. By varying α between α_c and 90°, v_{THz} can be adjusted between c and c/n, thereby allowing the synchronization between the particles and the accelerating field.

A practical choice for the dielectric medium is LN, since it has a large THz refractive index ($n \approx 5$) enabling synchronization to a wide range of proton energies. However, the most important advantage of LN is that the accelerator structure can be easily and efficiently

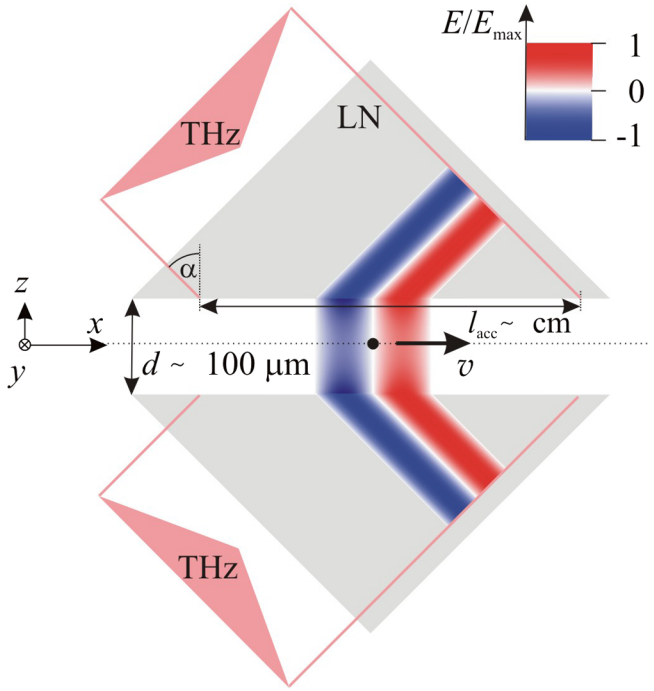

FIG. 1. Scheme of the THz-driven evanescent-wave postaccelerator.

combined with the THz source by using the same two pieces of LN both for TPFP as well as for evanescent-field generation. By using optimal pump pulse duration for THz generation, and cooling LN to 10 K (which reduces its THz absorption) single-cycle THz pulses with peak electric fields exceeding 2.6 MV/cm can be expected directly (i.e. without focusing) from a LN based TPFP source [23]. Using the Fresnel formula, this means an $E_{\mathrm{in},0} = 1.56$ MV/cm value inside the crystal with corresponding peak intensity of 3.2×10^{10} W/cm^2. Throughout the calculations, this value was assumed for the in-crystal field amplitude when the evanescent field was determined, and $\omega/2\pi = 0.5$ THz was assumed for the frequency (unless mentioned otherwise). For the sake of simplicity, the incoming THz pulse was supposed to be consisting of a single-cycle sine oscillation: $\mathbf{E}_{\mathrm{in}}(\mathbf{r},t) = \mathbf{E}_{\mathrm{in},0}\sin(\omega t - \mathbf{kr}) \times f(\omega t - \mathbf{kr})$, where $f(\varphi) = 1$ if $0 \le \varphi \le 2\pi$, and 0 otherwise. We note that in this case the Lawson-Woodward theorem [25] does not apply, since the interaction between the particle and the THz field is restricted to a finite region, because of the finite length of the crystal. Furthermore, the dispersion of LN is sufficiently low to avoid any significant distortion of the THz pulse over propagation of a few centimeters.

B. Acceleration of a single proton

In order to explore the maximum achievable proton energy boost, we first consider a single proton moving in the symmetry plane of the setup with initial velocity v_0 parallel to the x direction. In this plane the magnetic field vanishes and the electric field has only the longitudinal (x) component, which can be written as

$$E_x(x, z = 0, t) = E_0 \sin(\omega t - \kappa x + \phi_0) f(\omega t - \kappa x + \varphi_0), \tag{2}$$

with $\kappa = nk\sin\alpha$, and $E_0 = E_{\mathrm{in},0}[2\tau\xi\exp(-kd\xi/2)]/[1-\rho\exp(-kd\xi/2)]$. Let $v(t)$ denote the velocity of the particle, and $\varphi(t) = \omega t - \kappa x(t) + \varphi_0$ the phase of the field at the location of the particle, where ϕ_0 is the phase of the accelerating field at the position and time where and when the particle enters into the accelerator. The equation of motion is the following:

$$\frac{\mathrm{d}p}{\mathrm{d}t} = \frac{\mathrm{d}}{\mathrm{d}t}\left(\frac{mv}{\sqrt{1 - v^2/c^2}}\right) = qE_0 \sin(\varphi). \tag{3}$$

By applying $\mathrm{d}p/\mathrm{d}t = (\mathrm{d}p/\mathrm{d}v)(\mathrm{d}v/\mathrm{d}\varphi)(d\varphi/dt)$, and taking into account $\mathrm{d}\varphi/\mathrm{d}t = \omega(1 - v/v_{\mathrm{THz}})$ Eq. (3) can be rewritten as

$$(v - v_{\mathrm{THz}})\left(1 - \frac{v^2}{c^2}\right)^{-\frac{3}{2}} \frac{\mathrm{d}v}{\mathrm{d}\varphi} = a v_{\mathrm{THz}} \sin(\varphi), \tag{4}$$

where $a = qE_0/\omega m$ differs from the normalized vector potential only in a factor of c [26]. The form of Eq. (4) allows one to determine the particle's final velocity directly from the experimentally important (and easily controllable) phase parameters rather than having to consider the detailed temporal evolution of it. The solution of Eq. (4) gives for the final velocity of the particle

$$v(\phi;\phi_0) = \frac{c^4 v_{\mathrm{THz}} \pm \sqrt{g^4c^2 + g^2c^4v_{\mathrm{THz}}^2 - g^2c^6}}{c^2 v_{\mathrm{THz}}^2 + g^2}, \tag{5}$$

where

$$g(\phi;\phi_0) = \frac{c^2 - v_0 v_{\mathrm{THz}}}{\sqrt{c^2 - v_0^2}} c + a v_{\mathrm{THz}}[\cos(\phi_0) - \cos(\phi)]. \tag{6}$$

It is obvious that the maximal work can be extracted from the THz pulse if the particle passes through the entire positive half cycle of the sine wave twice (back and forth) as it is shown by the thick solid curve of Fig. 2. Please notice that there is a v^*_{THz} threshold THz velocity value (see Fig. 2). If $v_{\mathrm{THz}} < v^*_{\mathrm{THz}}$ the particle is continually accelerated along a trajectory shown by the thick dashed line in Fig. 2. If $v_{\mathrm{THz}} > v^*_{\mathrm{THz}}$ the acceleration ceases at the $\varphi = 0$ position, and the particle drops out of the pulse, as indicated by the thick dotted line in Fig. 2. If $v_{\mathrm{THz}} = v^*_{\mathrm{THz}}$ the particle travels through the $\phi = \pi \to \phi = 0 \to \phi = \pi$ trajectory (thick solid line in Fig. 2). v^*_{THz} can be determined by making equal v_{THz} with the velocity $v(\phi;\phi_0)$ given by

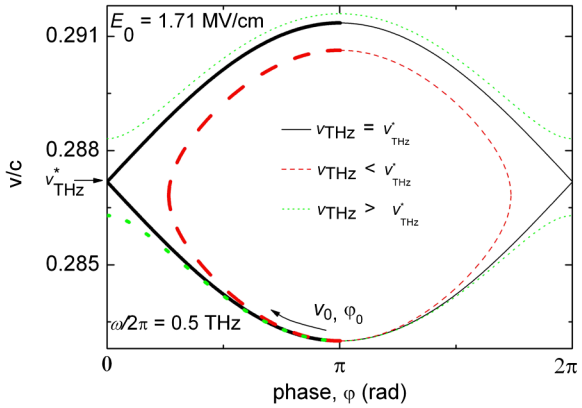

FIG. 2 . Proton velocity vs phase ϕ for $v_{\mathrm{THz}} = v^*_{\mathrm{THz}}$ (solid line), $v_{\mathrm{THz}} < v^*_{\mathrm{THz}}$ (dashed line), and $v_{\mathrm{THz}} > v^*_{\mathrm{THz}}$ (dotted line) THz phase velocities. The interaction within one half cycle of the field is shown by the thick part of the curves.

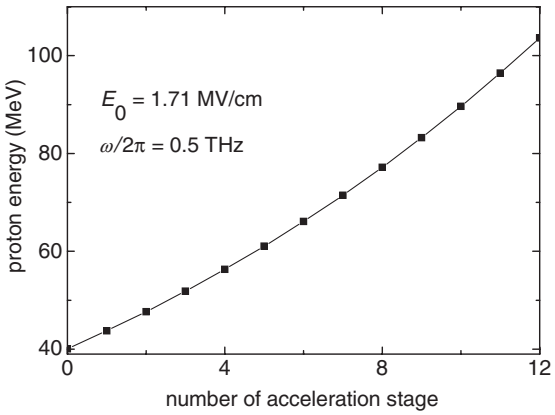

FIG. 3. Proton energies after subsequent units of a 12-stage accelerator sequence.

Eq. (5) for $\varphi = 0$; $\varphi_0 = \pi$. It is important to note that although the energy gain is maximal if $v_{\mathrm{THz}} = v^*_{\mathrm{THz}}$, the interaction length becomes infinite, which is impractical. Furthermore, the $\varphi = 0$ state is unstable. As an example we consider the acceleration of a single proton with 40 MeV initial energy ($v_0 = 0.283 \times c$). In this case $v^*_{\mathrm{THz}} = 0.2871 \times c$, and $v_{\mathrm{THz}} \approx v^*_{\mathrm{THz}}$ can be achieved by setting the incidence angle of the THz beam to $\alpha = 45.63°$; the initial phase can be set by delaying the TPFP pump pulse. The accelerating electric field amplitude in the $z = 0$ plane with $d = 50$ μm vacuum gap becomes $E_0 = 1.71$ MV/cm (see also Section II A). Obviously, the maximal proton energy gain (about 2.6 MeV) can be reached when $v_{\mathrm{THz}} \approx v^*_{\mathrm{THz}}$ (thick solid line in Fig. 2).

This requires an acceleration length of 2.8 cm, which can be set by choosing an appropriate beam diameter for the incoming THz fields. In the case of larger interaction length, the proton enters the deceleration regime (thin solid line). If $v_{\mathrm{THz}} < v^*_{\mathrm{THz}}$, the maximum proton energy gain is reduced (dashed line). If $v_{\mathrm{THz}} > v^*_{\mathrm{THz}}$, the proton gets dropped out of the THz pulse at $\phi = 0$ even before reaching $v = v^*_{\mathrm{THz}}$ (dotted line). We note that the structure of the phase diagrams is similar to the well-known separatrix used in the field of free-electron lasers [27]. We also note that at 0.25 THz frequency the vacuum gap was set to the more practical value of $d = 100$ μm, and the electric field amplitude has to be $E_0 = 0.7$ MV/cm in order to extract the same energy from the pulse as at 0.5 THz considered above.

Efficient acceleration requires centimeter-scale distances. As a consequence, for oblique incidence required by synchronization, the THz propagation length inside LN can vary by several centimeters across the beam. Material dispersion could cause a significant nonuniform lengthening of the single-cycle THz pulse, thereby continuously reducing the field amplitude along the acceleration length and hindering efficient energy transfer to the proton. As a simple estimate, the difference between phase and group delays gives a lower limit on the pulse length. In our above example this difference is only 0.7 ps, which is shorter than the typical length of (near-)single-cycle THz pulses. Therefore, dispersion effects were neglected here.

C. Multistage acceleration

The optimization described in Sec. II B gives the way to extract the maximum energy from a THz pulse. In order to achieve a significantly higher-proton-energy gain sufficient for hadron therapy the sequential arrangement of such accelerator units is needed. Please note that staging also provides a means to particle-field synchronization during a high-energy-gain acceleration process. Figure 3 shows the calculated output proton energy for a sequence of 12 accelerator stages. For the first stage the initial proton energy was 40 MeV. In each stage, the THz phase velocity was adjusted to the actual incoming proton energy. A stage-to-stage increase of the proton energy gain can be observed. The superlinear behavior can be explained by the increase in interaction length with increasing input velocity. For example, after the seventh stage the proton energy reaches 70 MeV, which can already be sufficient for certain hadron therapy applications. After stage 12, the 100-MeV energy level can be reached.

III. ACCELERATION OF PROTON BUNCHES

In Sec. II the acceleration of a single particle moving in the symmetry plane of the THz evanescent-wave accelerator was analyzed. However, it is of major practical importance to describe the motion of a particle bunch. Our General Particle Tracer simulations show that in the case of a proton bunch with typical spatial dimensions and $\sim 10^5$ proton number [8], the space charge effect is negligible, while in the case of bunches under the circumstances given in Ref. [3] with $\sim 10^{13}$ proton number it is significant. Our simulations show that in the case of a proton bunch with a typical size, the space charge effect has significance only

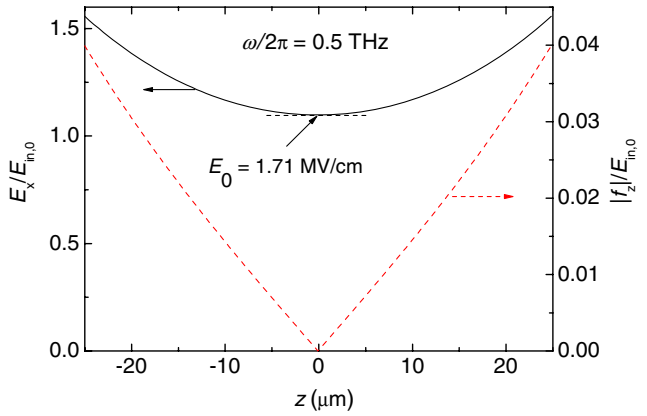

FIG. 4 . The longitudinal component of the electric field (solid line), and the absolute value of the transversal focusing/defocusing force acting on a unit charge (dotted line) vs the transversal coordinate. Please notice the more than one order of magnitude difference between the left and right scales.

above $\sim 10^7$ proton number. Proton bunches with $\sim 10^7$ particles can deliver the necessary dose for hadron therapy within a few minutes if 10 Hz repetition rate is assumed [1]. Therefore, in the following discussion, the Coulomb interaction is neglected when the motion of the particles in the external THz field is described.

Besides the longitudinal electric field component, for a particle bunch it is also necessary to take into account the transversal electromagnetic force given by $F_z = q(E_z - vB_y)$, which can lead to focusing or defocusing effects in the proton beam. The amplitude of the accelerating longitudinal electric field component E_x, and the absolute value of the amplitude of the transversal force acting on a unit charge $f_z = |F_z/q|$ are plotted versus the transversal coordinate in Fig. 4 for the case of a symmetric structure with the same parameters mentioned in Sec. II. We note that F_z is by 90° out of phase relative to the longitudinal force, since both E_z and B_y are by the same amount out of phase relative to E_x. As the particle leaves the phase belonging to the maximal longitudinal accelerating forces the transversal force starts to focus or defocus the particle beam.

A. Monochromatization and transversal-field effects

In course of the model calculations a proton bunch with uniform energy distribution spanning the 40.1–41.6 MeV range was assumed, corresponding to a high-energy narrow-band slice of a typical LDPA proton beam. It was assumed, that each of the $N = 100$ considered protons leave the LDPA simultaneously. The distance of the evanescent accelerator from the LDPA was set such that the slowest ($i = 1$) and fastest ($i = 100$) proton should reach the accelerator with a time delay equal to half of the THz oscillation period. For 0.5 THz frequency this condition limits the distance to 5 mm. Since LDPA proton beams typically have a relatively large divergence, this short distance allows coupling the beam efficiently into the THz-driven postaccelerator. On the other hand, although at this distance the intensity of the LDPA driving laser decreases typically by 4 orders of magnitude, it can damage the dielectric prisms. In the future when a more detailed design of such a postaccelerator setup is done, this danger has to be taken into consideration.

For applications in hadron therapy, monoenergetic proton beams with high energy are required. Therefore, besides boosting the proton energy, another important goal is the monochromatization of the energy spectrum. Our calculations show that by adequate setting of the parameters v_{THz}, φ_0, and the acceleration length l_{acc} it is possible to achieve that most of the particles leave the accelerator with about the same energy. In Fig. 5, the initial and output energies can be seen for each proton corresponding to parameters $v_{\mathrm{THz}} = 0.2871 \times c$, $\phi_0 = 3$ rad for the slowest ($i = 1$) particle, and $l_{\mathrm{acc}} = 1.25$ cm. The latter value gives a good compromise between maximizing the average energy gain and achieving a high degree of monochromatization. For comparison, as it was mentioned in Sec. II, $l_{\mathrm{acc}} \approx 2.8$ cm would be required to maximize the proton energy. As it can be seen in Fig. 5, about 50% of the accelerated protons have an energy which falls within ±0.25% of the 42.37 MeV mean energy.

The transversal motion of the particles, which could lead to beam focusing or defocusing, was also analyzed. The transversal force is zero in the symmetry plane and increases with the distance from the plane (Fig. 4). It was also taken into consideration that the transversal force is by 90° out of phase relative to the longitudinal force. As an example, the curves in Fig. 6 represent the transversal motion of three particles during the acceleration process, which belong to the beginning ($i = 20$), to the middle ($i = 40$) , and to the end ($i = 60$) of the plateau in Fig. 5. In order to consider the most pessimistic case, it was assumed in the calculations that each proton is at the edge

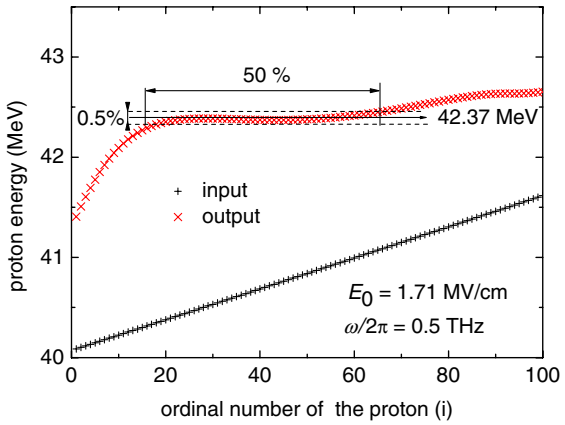

FIG. 5 . Input (+) and output (×) energy distribution for a proton bunch.

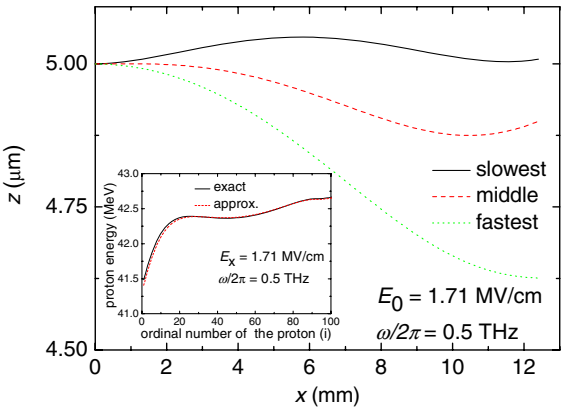

FIG. 6 . Trajectory of protons with initial transversal offset. The inset shows the longitudinal velocity distribution when transversal forces are taken into account (solid line), and when they are neglected (dashed line).

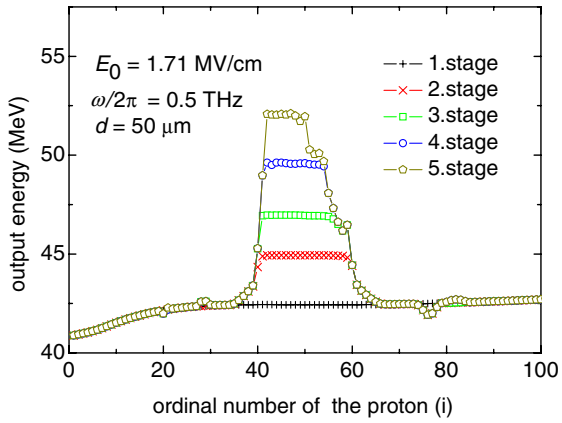

FIG. 7 . Output proton energy distributions for the subsequent stages of a five-stage accelerator sequence in the case of 0.5 THz frequency.

($z = 5$ μm) of the proton beam with a typical diameter of 10 μm when they reach the accelerator. As is evident from Fig. 6, the focusing effect is dominating rather than defocusing, and the variation of the z coordinate remains below 8% for each particle during the entire acceleration process. The inset of Fig. 6 shows that the transversal motion has no significant effect on the distribution of the longitudinal velocity component at the accelerator output. Very good coincidence is found between the curve belonging to the realistic case, when both longitudinal and transversal forces are present (solid line) and the curve belonging to the case, when particles move in the symmetry plane without any transversal force (dashed line).

B. Multistage acceleration of proton bunches

Multistage acceleration of proton bunches was also investigated. The strongly reduced energy spread of a large part of the protons in the bunch (Fig. 5) gives the possibility of putting the second accelerator significantly further (in the simulations 30 cm) away from the first. This enables one to use compact insertion devices (e.g. a miniature quadrupol magnet doublet) for collimating the proton beam [28,29], allowing for the transmission of a large part of the protons through the gaps of a large number of acceleration stages. The more technical details of using insertion devices is not a subject of the present paper. For each stage the parameters were set to obtain a good compromise between monochromatization and energy gain. For the sake of simplicity, the transversal motion was neglected. Results of acceleration in five steps are shown in Fig. 7.

It can be seen that the ratio of monochromatized particles decreases with the number of the stage, but even behind the fifth stage still ~10% of the originally considered particles fall into the ±0.35% range of the 52 MeV mean energy.

Additional improvement can be achieved in terms of both energy gain and monochromatization if a longer THz wavelength is used. Figure 8 shows the results obtained for

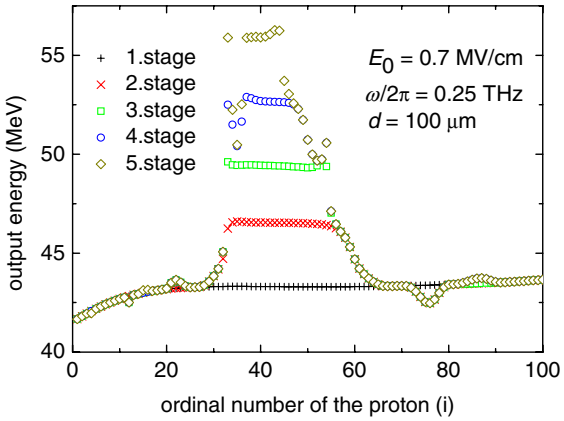

FIG. 8 . Output proton energy distributions for the subsequent stages of a five-stage accelerator sequence in the case of 0.25 THz frequency.

0.25 THz frequency. Comparison with Fig. 7 shows that the 56 MeV average energy in the fifth stage is significantly larger than the 52 MeV obtained for 0.5 THz. Similarly to the 0.5 THz case 10% of the particles fall into the ±0.35% range of the peak energy in the fifth stage. One important advantage of the longer THz wavelength is that it allows one to have a wider vacuum gap between the LN blocks.

We note that the proposed method can be applied for the acceleration of ions (e.g. carbon) as well, provided that synchronization between the particle and the accelerating field can be realized. This requires the initial velocity of the ions to be in the range between c and c/n. Naturally, for ions this means larger input energy than for protons.

IV. SUMMARY

An evanescent-field proton accelerator driven by single-cycle, high-field and high-energy THz pulses was proposed and analyzed. The main advantage of the THz-driven

accelerator is that the 0.1–0.5 THz frequency range naturally fits in wavelength to practical sizes of proton beams generated in laser-driven proton accelerators. Since the same laser pulse can be used to drive the LDPA as well as the THz source, high-precision synchronization between the accelerating field and incoming particle is inherently fulfilled. A practical realization of the setup is made up of a vacuum gap between two symmetrically arranged LN prisms. This allows one to combine both TPFP THz source and evanescent-field generation into a single pair of LN blocks, thereby leading to a very compact setup.

A simple model was used for analyzing and optimizing the acceleration of a single proton by the single-cycle evanescent field. Conditions for the highest proton energy gain were given. It was shown by numerical calculations that a quasimonoenergetic proton bunch can be generated by simultaneously increasing the proton energy. In order to reach the necessary energy, the accelerator stages can be used sequentially, thereby also allowing the precise adjustment of the synchronization during the acceleration process. As an example, it was shown that the energy of a 40 MeV proton bunch can be boosted by 28% in a five-stage accelerator sequence, and a simultaneous monochromatization of the energy distribution can be achieved resulting in a smaller than 1% energy deviation for 10% of the protons.

It is important to note that since the investigation of the proposed postaccelerator device is in an initial state, there is need for more accurate and detailed modeling in the future. The proposed method holds promise to contribute to the realization of compact and flexible hadron therapy machines, as well as to enable other applications for LDPAs requiring narrow-energy-spread proton beams.

ACKNOWLEDGMENTS

Financial support from Hungarian Scientific Research Fund Grant No. K101846, from the National Development Agency Grant No. ELI_09-1-2010-0013, and SROP-4.2.2.A-11/1/KONV-2012-0065 is acknowledged.

[1] U. Linz and J. Alonso, Phys. Rev. ST Accel. Beams **10**, 094801 (2007).

[2] U. Amaldi, *EuCARD Newsletter* ***3*** *(2010) [http://eucard-old.web.cern.ch/eucard-old/news/newsletters/issue03/article4.html].*

[3] R. A. Snavely, M. H. Key, S. P. Hatchett, T. E. Cowan, M. Roth, T. W. Phillips, M. A. Stoyer, E. A. Henry, T. C. Sangster, M. S. Singh, S. C. Wilks, A. MacKinnon, A. Offenberger, D. M. Pennington, K. Yasuike, A. B. Langdon, B. F. Lasinski, J. Johnson, M. D. Perry, and E. M. Campbell, Phys. Rev. Lett. **85**, 2945 (2000).

[4] J. Fuchs, P. Antici, E. D'Humieres, E. Lefebrve, M. Borghesi, E. Brambrink, C. A. Cecchetti, M. Kaluza, V. Malka, M. Manclossi, S. Meyroneinc, P. Mora, J. Schreiber, T. Toncian, H. Pépin, and P. Audebertl, Nat. Phys. **2**, 48 (2006).

[5] L. Robson, P. T. Simpson, R. J. Clarke, K. W. D. Ledingham, F. Lindau, O. Lundh, T. McCanny, P. Mora, D. Neely, C.-G. Walström, M. Zepf, and P. McKenna, Nat. Phys. **3**, 58 (2007).

[6] A. Heig, D. Kiefer, K. Markey, D. C. Gautier, K. A. Flippo, S. Letzring, R. P. Johnson, T. Shimada, L. Yin, B. J. Albright, K. J. Bowers, J. C. Fernandez, S. G. Rykovanov, H.-C. Wu, M. Zepf, D. Junk, V. Kh. Liechtenstein, J. Schreiber, D. Habs, and B. M. Hegelich, Phys. Rev. Lett. **103**, 045002 (2009).

[7] R. Prasad, A. A. Andreev, S. Ter-Avetisyan, D. Doria, K. E. Quinn, L. Romagnani, C. M. Brenner, D. C. Caroll, N. P. Dover, D. Neely, P. S. Foster, P. Gallegos, J. S. Green, P. McKenna, Z. Najmudin, C. A. J. Palmer, J. Schreiber, M. J. V. Streeter, O. Tresca, M. Zepf, and M. Borghesi, Appl. Phys. Lett. **99**, 121504 (2011).

[8] D. Haberberger, S. Tochitsky, F. Fiuza, C. Gong, R. A. Fonseca, L. O. Silva, W. B. Mori, and C. Joshi, Nat. Phys. **8**, 95 (2012).

[9] S. Ter-Avetisyan, M. Schnürer, R. Polster, P. V. Nickels, and W. Sandner, Laser Part. Beams **26**, 637 (2008).

[10] M. Schollmeier, S. Becker, M. Geissel, K. A. Flippo, A. Blazevic, S. A. Gaillard, D. C. Gautier, F. Grüner, K. Harres, M. Kimmel, F. Nürnberg, P. Rambo, U. Schramm, J. Schreiber, J. Schütrumpf, J. Schwarz, N. A. Tahir, B. Atherton, D. Habs, B. M. Hegelich, and M. Roth, Phys. Rev. Lett. **101**, 055004 (2008).

[11] O. Willi, T. Toncian, M. Borghesi, J. Fuchs, E. D'Humieres, P. Antici, P. Audebert, E. Brambrink, C. Cecchetti, A. Pipahl, and L. Romagnani, Laser Part. Beams **25**, 71 (2007).

[12] T. Toncian, M. Borghesi, J. Fuchs, E. D'Humieres, P. Antici, P. Audebert, E. Brambrink, C. A. Cecchetti, A. Pipahl, L. Romagnani, and O. Willi, Science **312**, 410 (2006).

[13] P. Antici, M. Migliorati, A. Mostacci, L. Picardi, L. Palumbo, and C. Ronsivalle, Phys. Plasmas **18**, 073103 (2011).

[14] P. Antici, M. Migliorati, A. Mostacci, L. Picardi, L. Palumbo, and C. Ronsivalle, J. Plasma Phys. **78**, 441 (2012).

[15] B. R. Fradsen, S. A. Glasgow, and J. B. Peatross, Laser Phys. **16**, 1311 (2006).

[16] T. H. Koschmieder, *Part. Accel.* ***48****, 75 (1994).*

[17] J. Hebling, G. Almási, I. Z. Kozma, and J. Kuhl, Opt. Express **10**, 1161 (2002).

[18] A. G. Stepanov, J. Kuhl, I. Z. Kozma, E. Riedle, G. Almási, and J. Hebling, Opt. Express **13**, 5762 (2005).

[19] A. G. Stepanov, S. Henin, Y. Petit, L. Bonacina, J. Kasparian, and J.-P. Wolf, Appl. Phys. B **101**, 11 (2010).

[20] J. A. Fülöp, L. Pálfalvi, S. Klingebiel, G. Almási, F. Krausz, S. Karsch, and J. Hebling, Opt. Lett. **37**, 557 (2012).

[21] S.-W. Huang, E. Granados, W. R. Huang, K.-H. Hong, L. E. Zapata, and F. X. Kärtner, Opt. Lett. **38**, 796 (2013).

[22] H. Hirori, A. Doi, F. Balanchard, and K. Tanaka, Appl. Phys. Lett. **98**, 091106 (2011).

[23] J. A. Fülöp, L. Pálfalvi, G. Almási, and J. Hebling, Opt. Express **19**, 15090 (2011).
[24] L. Pálfalvi, J. A. Fülöp, G. Almási, and J. Hebling, Appl. Phys. Lett. **92**, 171107 (2008).
[25] E. Esarey, P. Sprangle, and J. Krall, Phys. Rev. E **52**, 5443 (1995).
[26] E. Esarey, C. B. Schroeder, and W. P. Leemans, Rev. Mod. Phys. **81**, 1229 (2009).
[27] P. Schmüser, M. Dohlus, and J. Rossbach, *Ultraviolet and Soft X-Ray Free-Electron Lasers* (Springer, Berlin, 2009).
[28] T. Eichner, F. Grüner, S. Becker, M. Fuchs, D. Habs, R. Weingertner, U. Schramm, H. Backe, P. Kunz, and W. Lauth, Phys. Rev. ST Accel. Beams **10**, 082401 (2007).
[29] M. Fuchs, R. Weingartner, A. Popp, Zs. Major, S. Becker, J. Osterhoff, I. Cortire, B. Zeitler, R. Hörlein, G. D. Tsakiris, U. Schramm, T. P. Rowlands-Rees, S. M. Hooker, D. Habs, F. Krausz, S. Karsch, and F. Grüner, Nat. Phys. **5**, 826 (2009).